T-wave generation and propagation: A comparison between data and spectral element modeling[a)]

Guillaume Jamet[b)] and Claude Guennou
Université de Brest, Laboratoire Domaines Océaniques (UMR6538), Institut Universitaire Européen de la Mer, Place Nicolas Copernic, 29280 Plouzané, France

Laurent Guillon
Ecole Navale, Institut de Recherche de l'École Navale, BCRM Brest - CC 600, 29240 Brest Cedex 9, France

Camille Mazoyer
Université de Brest, Unité Mixte de Service 3113, Institut Universitaire Européen de la Mer, Place Nicolas Copernic, 29280 Plouzané, France

Jean-Yves Royer
Centre National de la Recherche Scientifique, Laboratoire Domaines Océaniques (UMR6538), Institut Universitaire Européen de l Mer, Place Nicolas Copernic, 29280 Plouzané, France

(Received 29 September 2012; revised 31 July 2013; accepted 6 August 2013)

T-waves are underwater acoustic waves generated by earthquakes. Modeling of their generation and propagation is a challenging problem. Using a spectral element code—SPECFEM2D, this paper presents the first realistic simulations of T-waves taking into account major aspects of this phenomenon: The radiation pattern of the source, the propagation of seismic waves in the crust, the seismic to acoustic conversion on a non-planar seafloor, and the propagation of acoustic waves in the water column. The simulated signals are compared with data from the mid-Atlantic Ridge recorded by an array of hydrophones. The crust/water interface is defined by the seafloor bathymetry. Different combinations of water sound-speed profiles and sub-seafloor seismic velocities, and frequency content of the source are tested. The relative amplitudes, main arrival-times, and durations of simulated T-phases are in good agreement with the observed data; differences in the spectrograms and early arrivals are likely due to too simplistic source signals and environmental model. These examples demonstrate the abilities of the SPECFEM2D code for modeling earthquake generated T-waves.
 [http://dx.doi.org/10.1121/1.4818902]

PACS number(s): 43.30.Qd, 43.30.Ma, 43.30.Dr [JAC] Pages: 3376–3385

I. INTRODUCTION

The submarine seismic and volcanic activity in the ocean generates a large amount of low-frequency (below 40 Hz) acoustic waves that propagate in the water column over very large distances (beyond 1000 km). In this paper, we model the generation and propagation of such acoustic waves, using the numerical code SPECFEM2D based on a spectral element method. The simulations of an actual earthquake in the Atlantic Ocean with a solid/fluid layered medium with different seismic and sound velocity profiles are compared with hydroacoustic waves recorded few hundred kilometers away.

Seismic waves convert into acoustic waves at the sea bottom that in turn propagate in the water column and, at low frequencies (0–40 Hz; Williams *et al.*, 2006, Fig. 7), can be carried over very long distances with little attenuation in the sound fixing and ranging (SOFAR) channel. Earthquake generated acoustic waves in the ocean are referred to as T-waves (or tertiary waves) because in certain conditions, when they reach the shore, they may convert back to seismic waves and arrive third after the P- and S-seismic waves on near-shore seismological stations. Acoustic waves travel at 1500 m/s in the ocean whereas seismic P- and S-waves travel at velocities from 2000 to 7000 m/s in the crust. The first documented record of T-waves dates from 1927 (Jagger, 1930), but their origin was not linked to an earthquake until a decade later (Linehan, 1940). Then it is only after the Second World War that Tolstoy and Ewing (1950) presented the correct physics. Hydrophones, originally deployed to detect ships and submarines or to monitor biological sounds, are now currently used to record T-waves for monitoring the seismic and volcanic activity of the ocean floor (e.g., Fox *et al.*, 1994; Goslin *et al.*, 2005; Goslin *et al.*, 2008). Toward this goal, our laboratory collected a large set of acoustic data with hydrophone arrays in the Atlantic and Indian oceans. Due to the remarkable acoustic properties of the ocean, these arrays detect 10–30 times more earthquakes than land-based stations, particularly the low-magnitude events that are undetected on land due to the rapid attenuation of seismic waves in the Earth crust. The earthquakes are detected by analyzing the acoustic energy received by each hydrophone and the source of these T-waves can be accurately located by

[a)]Preliminary results of this work were presented in "Very low frequency wave propagation numerical modeling: Application to T-wave propagation," in *Proceedings of the 11th European Conference on Underwater Acoustics (ECUA)*, Edinburgh, UK, July 2012.

[b)]Author to whom correspondence should be addressed. Electronic mail: guillaume.jamet@univ-brest.fr

triangulating the arrival times of the maximum energy on each hydrophone (i.e., peak of the envelop). However, several questions arise. Does this location correspond to the earthquake epicenter or to a spot on the seafloor where the seismo-acoustic conversion is the most efficient, and how wide is this spot? What information can we learn from the recorded signals about the seismic event (magnitude, depth, focal mechanism) and about the media in which the waves have propagated? Answering these questions requires a better understanding of the mechanisms of generation and propagation of T-waves, i.e., understanding the conversion from seismic to acoustic waves and the effects of long-distance propagation of acoustic signals through the water column and SOFAR channel.

To address this challenging problem, this study uses the numerical code SPECFEM2D (Tromp *et al.*, 2008) based on a spectral element approach with model parameters as close as possible to a real setting: Source parameters from an actual earthquake and a medium including an oceanic crust layer and a water layer, where seismic and acoustic waves will propagate. Synthetic signals are then compared to acoustic records from an array of hydrophones. Section II presents the dataset used for comparison with the simulations; Sec. III presents different numerical methods for modeling T-wave propagation and the reasons for selecting the SPECFEM2D code. Section IV presents the model parameters and Sec. V a discussion of the results.

II. THE "MARCHE" HYDROACOUSTIC EXPERIMENT

The setting, model parameters and data used in this paper correspond to and are derived from the Mid-Atlantic Ridge Comprehensive Hydrophone Experiment (MARCHE; Goslin *et al.*, 2008). The purpose of this experiment was to monitor the low-level seismicity associated with seafloor-spreading processes along the mid-Atlantic Ridge. During this 3-yr long experiment, an array of four hydrophones was moored at a depth of 1000 m below sea-level, in the SOFAR channel, on either side the mid-Atlantic ridge, south of the Azores. The autonomous hydrophones were 600–800 km apart (Fig. 1) and set to record acoustic data continuously at

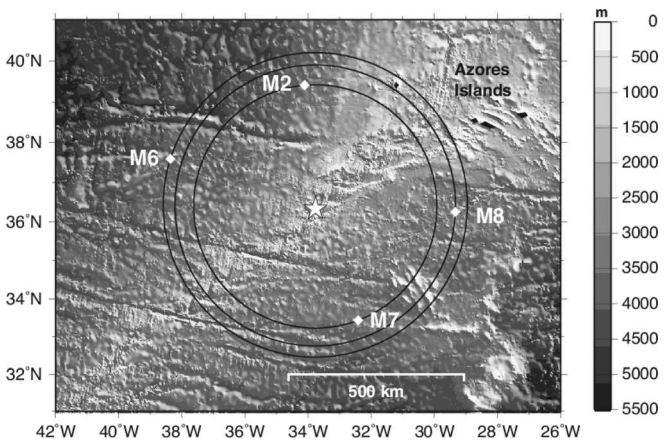

FIG. 1. Bathymetric chart of the mid-Atlantic Ridge, south of the Azores Islands, with the four hydrophones from the MARCHE experiment (white diamonds). The star shows the location of the March 2, 2008, earthquake.

a 250 Hz sampling rate. Between August 2005 and August 2008, more than 7400 earthquakes were detected and located (with a precision of about 2 km) along this section of the mid-Atlantic Ridge.

The earthquake modeled in this work occurred March 2, 2008 at 1h34m21.3 s GMT on the mid-Atlantic ridge axis, in the center of the MARCHE hydroacoustic array (Fig. 1). Its location (36.33°N; 33.77°W;), its magnitude (Mw = 5.1), source duration (1.8 s) and moment tensor [Eq. (1)] were determined from land-based seismic stations [Global Centroid-Moment-Tensor (CMT) Project; www.globalcmt.org]. The moment tensor, which describes the focal mechanism, is defined by a 3×3 symmetric matrix in which each element represents a couple. In Eq. (1), the **r**, **t**, and **p** axes are up, south, and east, respectively. The CMT location is only 5 km from that inferred from T-waves inversion (36.35°N; 33.82°W). Figure 2 shows acoustic records of this event at M6, M7, and M8 locations. Hydrophone M2 is unsuitable for comparisons due to an overloaded signal and a high level of noise.

$$M = \begin{pmatrix} M_{rr} & M_{rt} & M_{rp} \\ M_{rt} & M_{tt} & M_{tp} \\ M_{rp} & M_{tp} & M_{pp} \end{pmatrix} = \begin{pmatrix} -5.51 & 1.61 & 0.784 \\ 1.61 & 2.42 & 2.78 \\ 0.784 & 2.78 & 3.09 \end{pmatrix}_{(\mathbf{r},\mathbf{t},\mathbf{p})} \times 10^{16}\text{N.m.} \quad (1)$$

III. NUMERICAL MODELING

A. Analytical modeling of T-waves

Modeling T-wave generation and propagation has been the subject of numerous works since their discovery (see Okal, 2008, and references therein). Its complexity comes from the conversion of a seismic energy, which propagates nearly vertically up to the seafloor, into an acoustic energy that propagates nearly horizontally in the water column. Based on geometrical acoustics, it was first suggested that the conversion resulted from the incidence of the seismic rays relative to a sloping seafloor and to the multiple reflections of acoustic waves between the sea surface and a sloping seafloor that would bend the acoustic rays toward the horizontal until they reach a critical angle to propagate in the SOFAR. Acoustic rays were also used to explain multiple arrivals from a single earthquake by the conversion of seismic energy to acoustic energy at seamounts and ridges (Chapman and Marrett, 2006). This model highlighted the important fact that seismic to acoustic conversion does not occur on a single spot on the seafloor but on a more or less extended area and thus that the 3D geometry of the seafloor around the epicenter must be taken into account.

These models, however, fail to account for the generation of T-waves on abyssal (flat) plains. This difficulty has been dealt with by a modal description of sound propagation in the ocean (Park *et al.*, 1999). Low-order acoustic modes

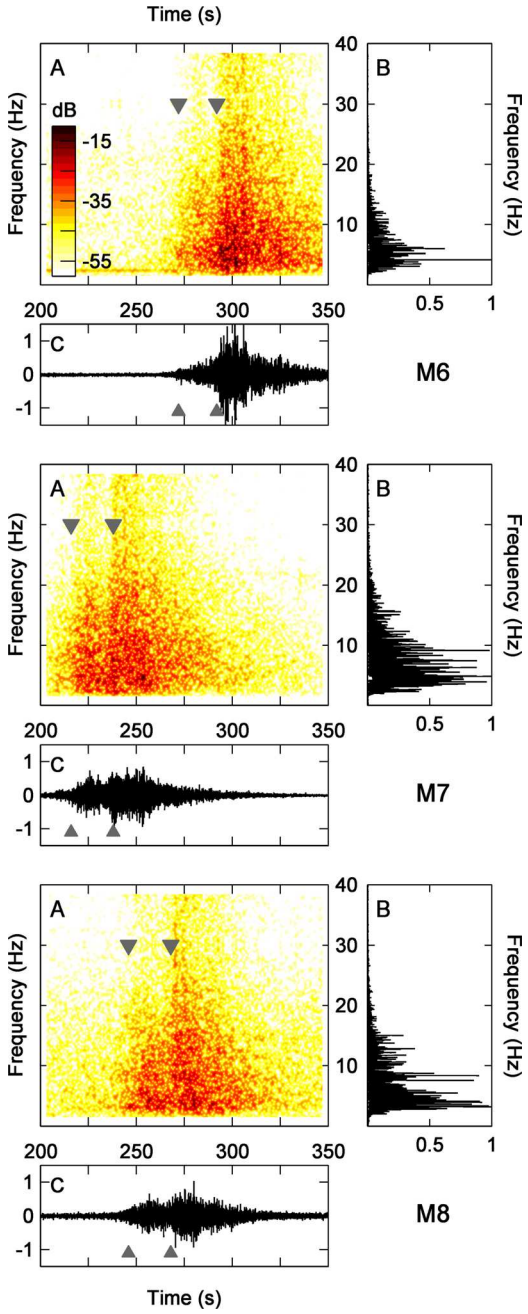

FIG. 2. (Color online) Hydroacoustic records of the March 2, 2008, earthquake at hydrophone locations M6, M7, and M8, respectively at 431, 347, and 398 km from the epicenter (star in Fig. 1). Arrows show the arrival times of high energy T-waves. For each hydrophone are shown the power spectrum in decibels (A), the amplitude spectrum (B) and the time signal normalized to peak level in M7 (C).

can propagate in the water column, but their amplitudes decrease quickly below the seafloor, and thus they cannot be excited by an earthquake. Conversely, high-order modes are excited at earthquake depths but do not propagate in the water column. This problem can be overcome by taking into account the range dependent nature of the propagating medium. Indeed, a sloping interface or a rough seafloor transfers energy from high- to low-order modes and thus allows an earthquake to generate acoustic wave in the water. Based on this idea (with different approximations), de Groot-Hedlin and Orcutt (2001) and Yang and Forsyth (2003) were for instance able to generate synthetic T-waves that realistically match recorded T-waves.

From this discussion, it appears clearly that the T-wave generation is a very complex phenomenon that involves several elements: Focal mechanism, velocities of P- and S-seismic waves in the upper crust, sound-speed profile in the water-column, multi-scale bathymetry. The main limitation of the analytical or semi-analytical approaches described in the preceding text is that they do not take into account all these parameters, and particularly the source parameters.

B. SPECFEM2D

Among numerical methods used to simulate seismic and acoustic wave propagation, we selected a spectral element method (SEM) to simulate numerically the propagation of T-waves. SEM is a high-order finite element method that combines the generality of a finite element method with the accuracy of spectral techniques. This method was first introduced by Patera (1984) for an application in fluid dynamics and further adapted by Komatitsch and colleagues for geophysical applications, in particular for large-scale seismic simulations (Komatitsch and Vilotte, 1998; Komatitsch and Tromp, 1999; Komatitsch *et al.*, 2000). Recently, SEM was also used to investigate underwater acoustic problems (Cristini and Komatitsch, 2012).

Our simulations are performed with the SPECFEM2D SEM-code (Tromp *et al.*, 2008). This code is able to simulate forward and adjunct coupled acoustic-(an)elastic wave propagation on arbitrary unstructured hexahedral meshes. SPECFEM2D is particularly well suited for modeling the generation and propagation of T-waves for several reasons. First it allows to model buried seismic sources as moment tensors located anywhere within the (an)elastic medium (which is a good approximation of the marine basement). Moment tensors are available from earthquake catalogs. Second, like all codes based on finite element method, SPECFEM2D is able to model complex (anelastic and/or inhomogeneous) media. Moreover it can numerically handle the problem of seismo-acoustic conversion at interfaces with an arbitrary geometry. This latter feature is particularly important for modeling T-waves because oceanic earthquakes mainly occur in areas with strongly varying bathymetry (ocean ridges, subduction zones). At the same time, unlike codes based on high-frequency ray-tracing approaches, SPECFEM2D is not frequency limited and can model the propagation of very low-frequency waves. Finally, time signals can be computed at any point of the mesh, which can be directly compared with observed waveforms.

IV. MODEL PARAMETERS

The objective is to set a model as close as possible to a real case to compare synthetic seismograms with actual acoustic records of the seismic event described in the Sec. II. Because our code is two-dimensional (2D), our simulation is done in the three vertical planes passing through the earthquake and each of the three hydrophones. Our model

includes a solid layer and a fluid layer separated by an interface derived from the seafloor bathymetry. The bathymetric profiles between the source and the receiver are extracted from the ETOPO1 global grid (1 arc min resolution, 1.50×1.85 km at 36°N; Amante and Eakins, 2009). The resolution of each profile depends on its orientation and the latitude but is in the same range as the original grid. These profiles are then input into SPECFEM2D, which computes the mesh. The size of the mesh is frequency dependent based on an empirical threshold of 5.5 points per wavelength to ensure computation stability. In our range of frequencies (4–15 Hz) and velocities (1.5–8.1 km/s), the mesh resolution ranges from ten to several ten of meters, which is two orders of magnitude smaller than the initial resolution. In addition, the mesh data are interpolated using a cubic spline function to avoid unwanted rugosity. The bathymetric profiles between the earthquake epicenter and hydrophones M6 and M7 cross ridges reaching the SOFAR channel axis whereas the epicenter-M8 hydrophone profile is always deeper than the SOFAR axis (Fig. 3). All models horizontally extend 10 km beyond the source and the receivers along the horizontal axis, and the solid layer has a constant thickness of 10 km meaning that its bottom boundary is parallel to the fluid/solid interface. This choice simplifies the simulation mesh and significantly speeds up the calculations. To avoid spurious reflections at the limits of the computation domain, its bottom, left, and right edges are modeled by absorbing layers, while the upper edge is a free surface. The source is located 8 km below the seafloor and is simulated by a Gaussian signal. The Gaussian shape is a common choice in the seismological community for approximating the temporal dependence of the strain created by earthquakes. For 2D simulations, the radiation pattern of the actual source, in the direction of a receiver, is obtained by projecting the 3D moment tensor [Eq. (1)] on the source-receiver vertical plane [Eq. (2)]

$$M6 = \begin{pmatrix} 4.8064 & -1.2899 \\ -1.2899 & -5.5100 \end{pmatrix} \times 10^{16}\text{N.m}$$

$$M7 = \begin{pmatrix} 4.4732 & -1.7872 \\ -1.7872 & -5.5100 \end{pmatrix} \times 10^{16}\text{N.m}$$

$$M8 = \begin{pmatrix} 3.1210 & 0.7930 \\ 0.7930 & -5.5100 \end{pmatrix} \times 10^{16}\text{N.m}. \quad (2)$$

It is worth noting that because an earthquake moment tensor is not spherical, the seismic source generates both compressional and shear waves. The resulting three radiation patterns are quite similar [Fig. 4 and Eq. (2)]: Compressional waves are preferentially emitted in almost vertical and horizontal directions and shear waves are emitted at 45° from these planes.

In all models, the density of the water is set at 1020 kg/m^3. The vertical sound speed profile is range-independent and is either considered as uniform (1495 m/s) or with a varying profile (Fig. 5). The sound-speed profile is an average profile for the area and for the month of March based on the generalized digital environmental model (GDEM; Teague *et al.*, 1990). The solid medium is modeled as a sequence of four layers, each layer having either a constant or linearly varying density and P- and S-wave velocities (Fig. 5). In the following, the former configuration is called a "stratified" model and the latter case is called a "gradient" model. The parameters for each layer are taken from the CRUST2.0 model (Bassin *et al.*, 2000). However our model neglects the thin low-velocity sediment layer (70-m-thick; $\rho = 1700$ kg/m^3; $v_p = 1800$ m/s and $v_s = 800$ m/s). The reasons are first to speed up the computation times because low seismic-velocities require very fine meshes and small time steps leading to much longer computation times and second because the study area is close to the ridge axis where sediments are very limited. The seismic attenuation in the solid medium is constant: $\alpha_p = 0.1$ dB/λ and $\alpha_s = 0.2$ dB/λ. The two water-sound profiles (constant vs gradient) and the two solid medium profiles (stratified vs gradient) yield four different models (Table I).

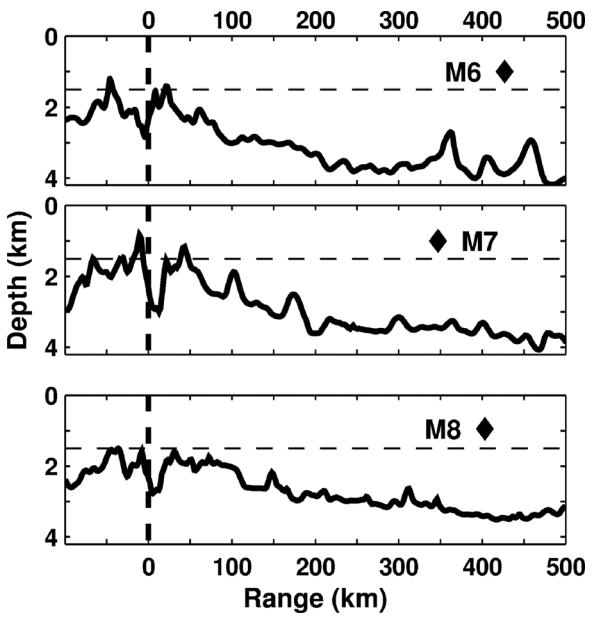

FIG. 3. Bathymetric profiles along the planes passing through the epicenter (vertical dashed line at 0 km) and the receivers (black diamonds). The horizontal dashed line corresponds to the depth of the SOFAR channel axis (Fig. 5).

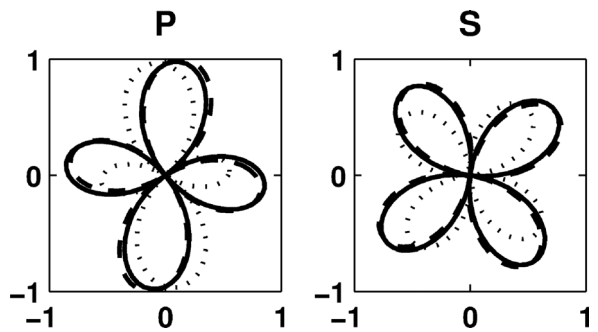

FIG. 4. Two-dimensional P- and S-wave radiation patterns of the source projected in the direction of M6 (solid), M7 (dashed), M8 (dotted) relative to the epicenter.

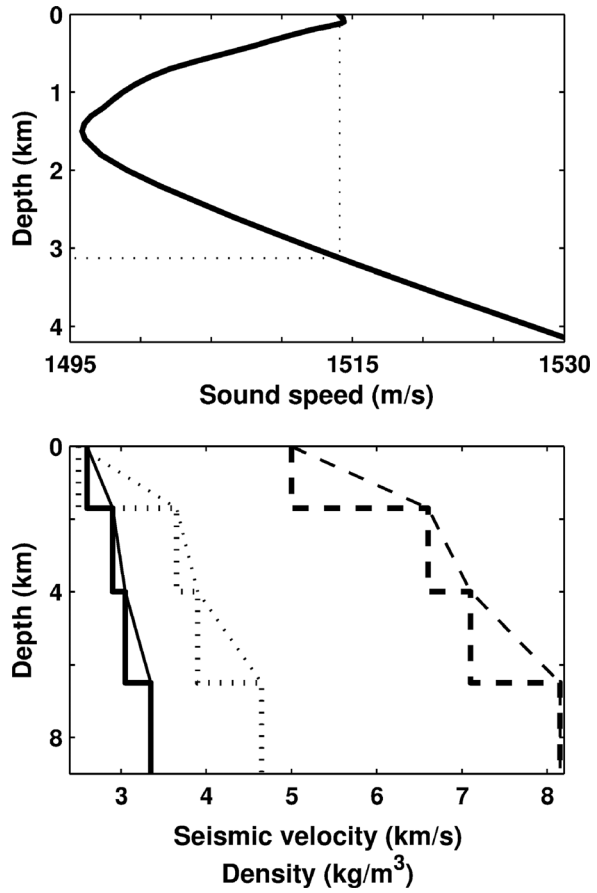

FIG. 5. Velocity profiles implemented in the water column (top) and the solid medium (bottom). In the water column, the sound-speed is either constant (1495 m/s) or changes with depth as shown. In the solid medium, stratified models consider stair-step increase (thick lines) in density (solid lines), S-wave (dotted lines) and P-wave (dashed lines) velocities, whereas models with a continuous gradient consider a gradual increase of these parameters with depth (thin lines).

All simulations use a Gaussian source signal with three different central frequencies. The seismic catalog gives a value of 1.8 s for the source signal duration, corresponding to a Gaussian signal with a central frequency of 0.55 Hz. With such source, the resulting T-phases have a frequency content much lower than that of the observed data (Jamet *et al.*, 2012). For this reason, we consider a source with a central frequency at 4 Hz, which is approximately the most energetic frequency in the observed T-wave spectra. Increasing this frequency requires more computing resources. The highest frequency allowed by our computing facilities for full-range simulations (up to 450 km) is 10 Hz and the longest horizontal range for which a 15 Hz Gaussian source signal can be tested is 200 km.

TABLE I. Different combinations of wave velocity profiles tested in the simulations (see Fig. 5).

Model name	Fluid layer	Solid layer
SG	SOFAR	Gradient
SS	SOFAR	Stratified
UG	Uniform	Gradient
US	Uniform	Stratified

V. RESULTS AND DISCUSSION

The different combinations of sources and velocity profiles are only tested for hydrophone M7, the closest from the earthquake epicenter (347 km) (Figs. 6, 7, 8, and 10). Only the most realistic environmental parameters and a source at 10 Hz are applied to simulate hydrophones M6 and M8 (case SG: SOFAR channel and a gradient model).

All simulations at the location of hydrophone M7 with a 4 Hz (Fig. 6) and a 10 Hz source (Fig. 7), and at 200 km range, in the direction of M7, with a 15 Hz source (Fig. 8), and at 100, 200, 300 km, in the direction of M7, with a 10 Hz source (Fig. 10) lead to the following observations.

Whatever the sound-speed profile considered in the water column (constant or with a low-sound velocity layer), differences between simulated signals are insignificant (Figs. 6–8). This observation stands for any particular choice of P- and S- wave velocity profiles in the solid medium or of a central frequency for the Gaussian source. In all simulations, the whole column is insonified by T-waves as illustrated in Fig. 9 in the particular case of "gradient" model in the solid layer, reflecting the fact that the SOFAR channel is as thick as the water column throughout the models.

Figure 10 and case SG of Fig. 7 show that, up to 347 km, the frequency content of the signal (B plots) from a same source (here at 10 Hz) varies little with the distance from the source, suggesting that the 15 Hz model, although limited at 200 km (Fig. 8), would be similar to a model at 347 km.

The frequency bandwidth of the simulated signals increases with the central frequency of the Gaussian source (Figs. 6–8). This is not surprising because the bandwidth of a Gaussian source is about an octave and will increase with the central frequency. The bandwidth (between half-power points) ranges from 2.8 to 5.6 Hz for 4 Hz source, from 7 to 14 Hz for a 10 Hz source, and from 10.6 to 21.2 Hz for a 15 Hz source. Further modeling of T-phases with this approach may help constraining the spectral width, dominant frequency, and duration of the actual source.

In addition, the spectrum amplitude is maximum at a frequency always lower than the central frequency of the source. This may partly be explained by the different units used for the source (a moment tensor expressed in N.m) and for the receiver (pressure expressed in N/m^2), as demonstrated, for example, in Appendix E of Stephen *et al.* (1985) in a purely acoustic case and in an homogeneous medium. Quantifying this effect in our model would be complicated by the presence of a solid/fluid interface between the source and the receiver.

The frequency content of the source is likely to be more complex than assumed by seismic land-based catalogs. The source duration is based on the recording of low-frequency seismic waves. A simple Gaussian-shaped source with a given duration of 1.8 s (i.e., 0.55 Hz) will be unable to reproduce the frequency range observed in the hydroacoustic data. As shown by our simulations, higher-frequency sources (i.e., with a shorter duration) provide a better match.

All simulations predict ~80 s long T-phase signals with a gradual increase in their amplitudes followed by a gradual

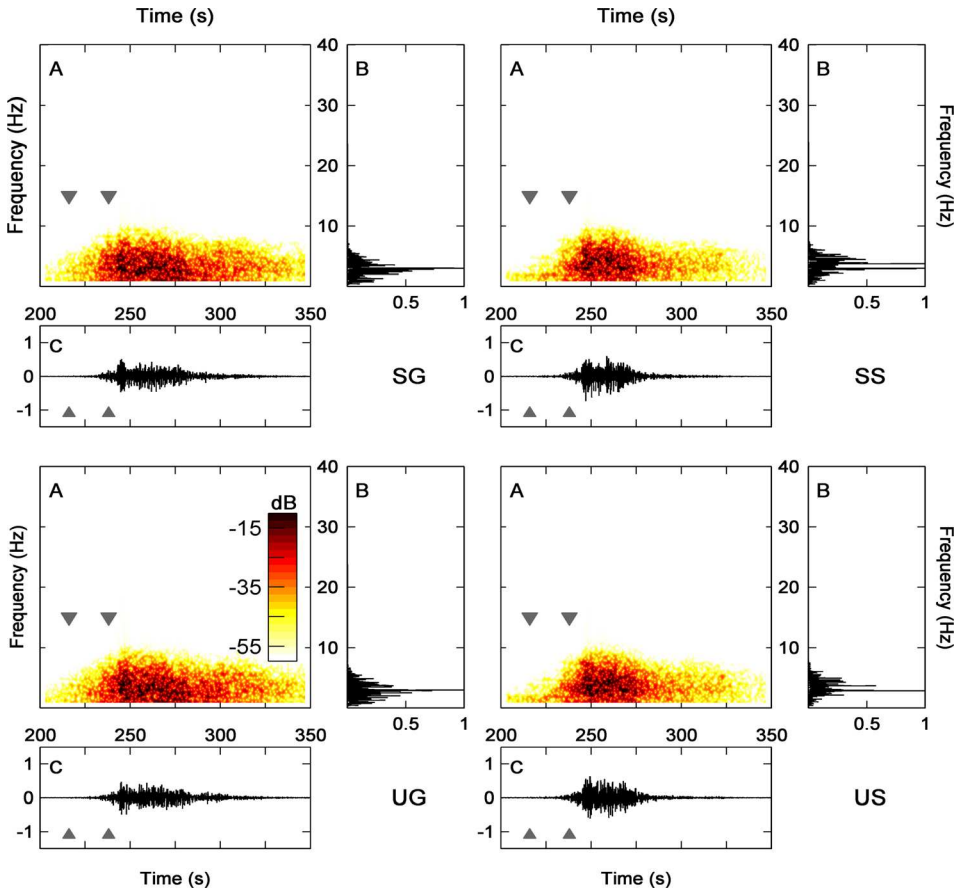

FIG. 6. (Color online) Simulated T-phase arrivals at hydrophone M7 (347 km), generated by a 4 Hz Gaussian seismic source. Each group of spectrogram (A), normalized spectrum (B), and time signal (C) corresponds to a combination (SG, SS, UG, US) of velocity profiles (see Table I). Data are shown with the same representation as Fig. 2. Arrows refer to T-wave arrival times in the actual data at M7 (Fig. 2).

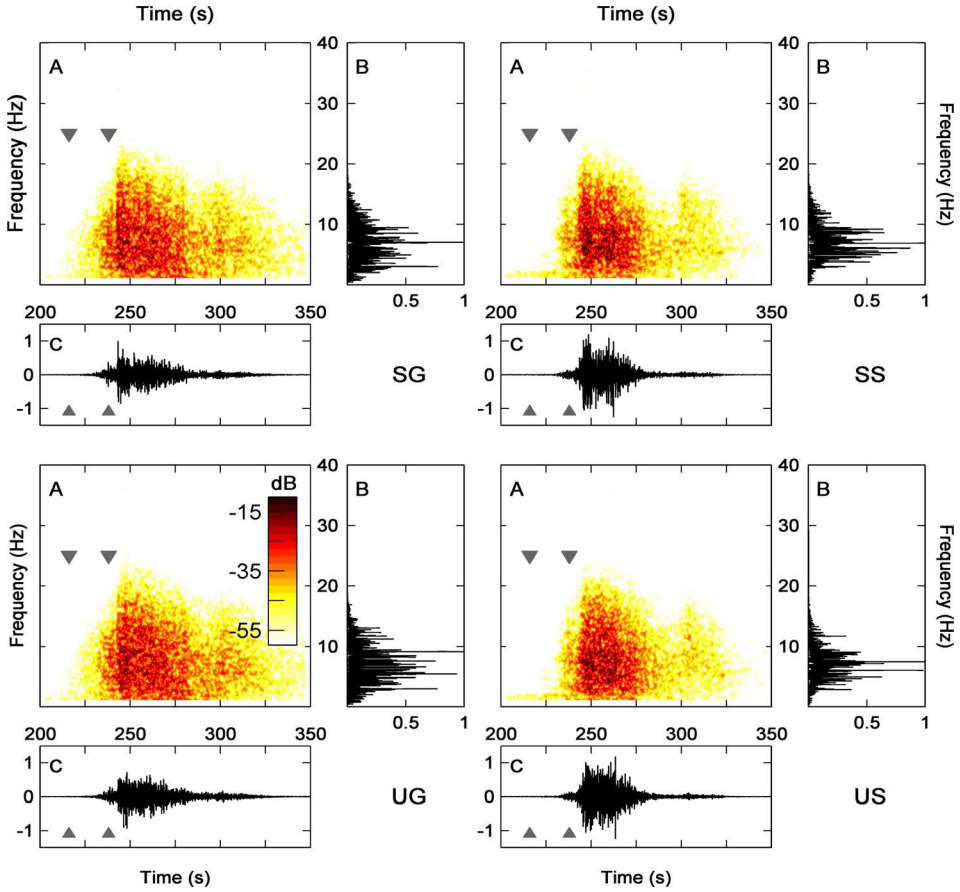

FIG. 7. (Color online) Simulated T-phase arrivals at hydrophone M7 (347 km), generated by a 10 Hz Gaussian seismic source. Same convention as in Fig. 6. Arrows refer to T-wave arrival times in the actual data at M7 (Fig. 2).

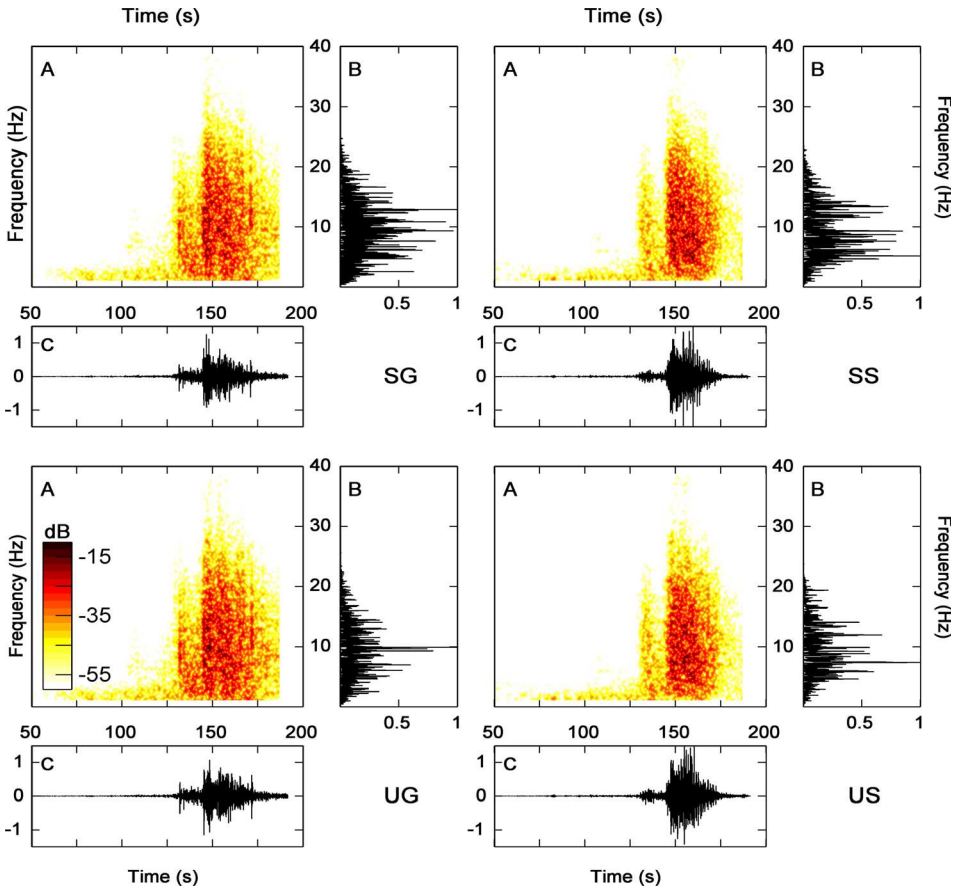

FIG. 8. (Color online) Simulated T-phase arrivals at a receiver 200 km away from the epicenter in the direction of M7, at the same depth as M7, and with a source at 15 Hz. Same convention as in Fig. 6.

decrease. However, synthetic T-wave signals have, in general, a shorter duration (∼80 s) than the observed T-waves (∼100 s); the signal length is even shorter with a stratified crustal model than with a continuous velocity gradient in the crustal layer.

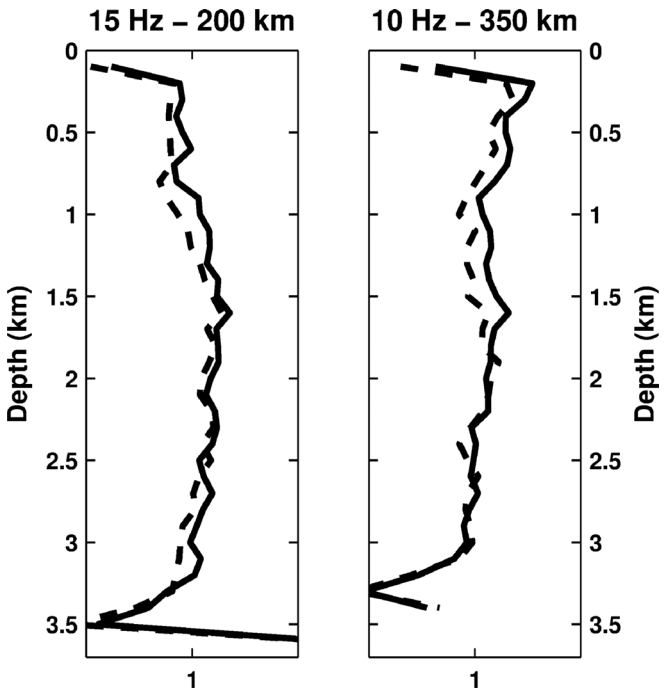

FIG. 9. Mean T-phase amplitude on a vertical array of receivers for models with a SOFAR channel (solid lines) or a uniform sound speed (dotted lines); both models consider a velocity gradient in the solid medium. Left and right models are, respectively, for receivers 200 and 350 km away from the epicenter, in the direction of M7, and for seismic sources at 15 and 10 Hz.

The synthetics at 10 Hz (Figs. 7 and 10) display distinct T-waves arrivals at short range (100 and 200 km) that tend to merge at longer range (300 and 347 km). In the model at 15 Hz (Fig. 8), these two distinct arrivals are even clearer and similar to that observed in the actual data (Fig. 2). These two arrivals (outlined with arrows in Fig. 2) are better seen in the spectrogram than in the time signal; the second and main arrival is expressed by a sudden increase in energy at all frequencies (up to 30 Hz) that occurs about 20 s after the first arrival. Spectrograms in Fig. 7 clearly display these two arrivals, the second after a 20 s delay and a frequency bandwidth twice as large as the initial arrival. In Fig. 10, the precursors and main arrivals are also clearly seen in the spectrograms and time signals; the delay between the two arrivals decreases as the range increases. In the simulations of all hydrophones (Fig. 11), the second energetic arrival matches pretty well the arrival-times observed in the actual data (arrows) with a slight delay (within 5 s). The precursor, or first arrival, is more subdued and delayed with respect to the actual first arrivals but is still visible (for M8 this delay reaches 15 s). Several factors may explain the weak first arrival and its delay relative to the observed early arrival at each hydrophone:

(1) Early arrivals may be due to the conversion of seismic waves away from the epicenter where the modeled topography of the seafloor is probably too smooth to produce efficient seismic/acoustic conversion (see discussion about the mesh description).

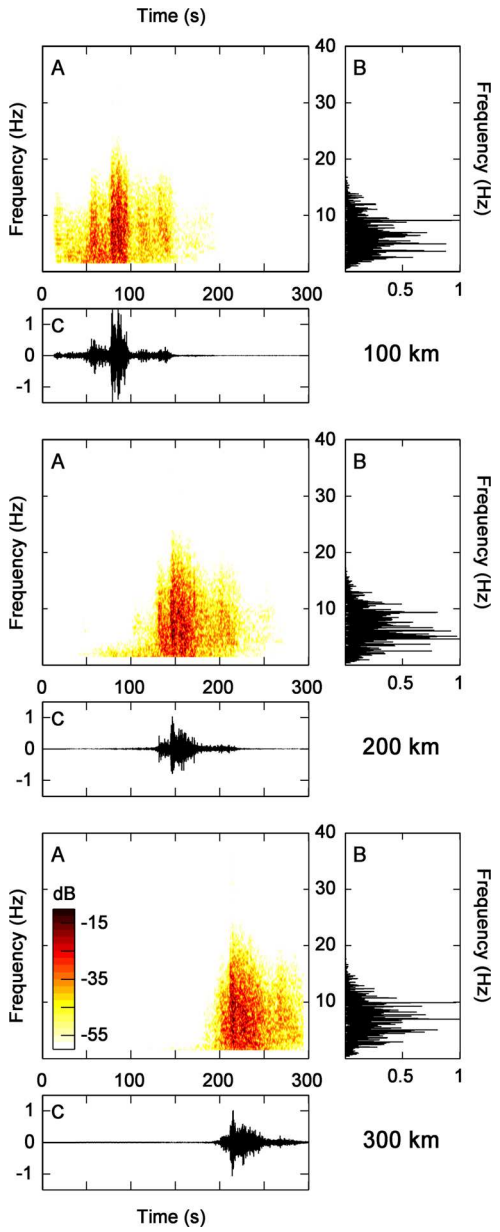

FIG. 10. (Color online) Simulated T-phase arrivals at receivers 100, 200, and 300 km away from the epicenter in the direction of M7, at the same depth as M7, and with a 10 Hz seismic source. All three models consider a SOFAR sound speed profile in the water column and a seismic velocity gradient in the solid medium. Same convention as in Fig. 6.

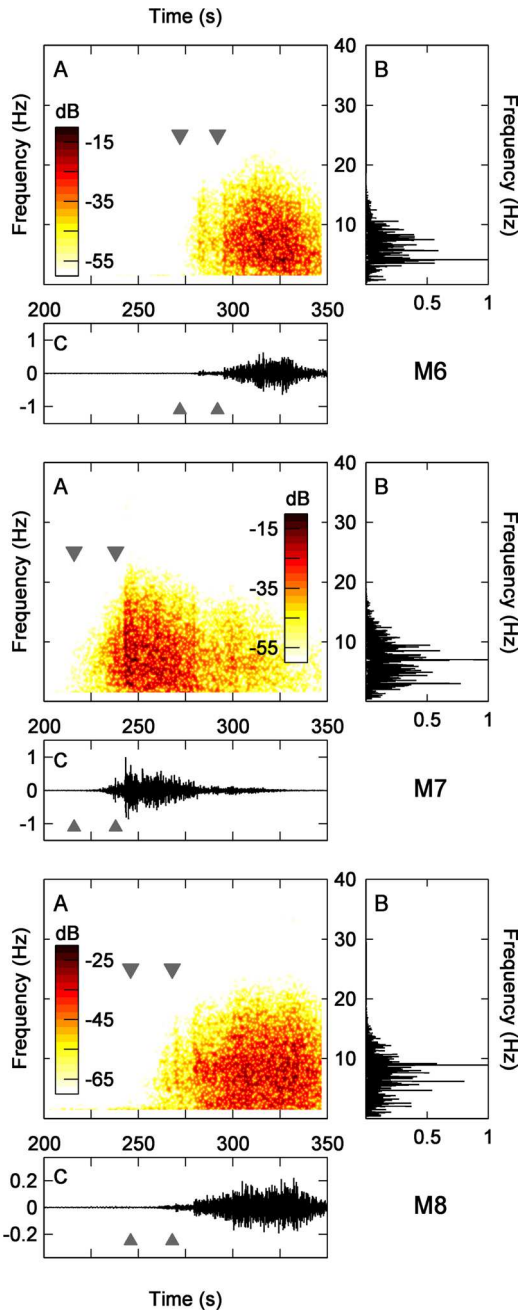

FIG. 11. (Color online) Simulated T-phase arrivals at hydrophones M6, M7, and M8 using a source at 10 Hz, a SOFAR sound speed profile in the water and a seismic velocity gradient in the crust. Arrows refer to T-wave arrival-times in the actual data (Fig. 2). Note that amplitude scales are enhanced for M8 (A and C plots). Same convention as in Fig. 6.

(2) The velocity structure of the crust is also assumed constant at all ranges and in all directions. Furthermore, the model does not take into account the sediment layer away from the ridge axis, which may alter the seismic/acoustic conversions away from the epicentral area.
(3) Errors in the location and depth of the source may account for few seconds in the observed delays. The source depth from teleseismic data is generally ill constrained. However, as pointed out earlier, the CMT and T-wave locations of the epicenter are less than 5 km apart. Close comparisons between T-wave and teleseismic wave localization of earthquakes have shown that the former are more accurate than the latter (e.g., Pan and Dziewonski, 2005). Furthermore, these inversions are generally based on the second and more energetic T-wave arrivals.
(4) Finally, we assume a constant sound-velocity profile in all directions and at all range; this may also partly account for the variable and small delays in the second P arrivals. These delay differences may thus be inherent to the approximations in the environmental parameters: First they assume a horizontal isotropy in the water and solid media, and second, the crust/water interface is probably too smooth, particularly in the epicentral area and lacks a sediment cover. The ability of our approach to produce such precursors opens new perspectives to

investigate their origin and propagation. Data comparable to the setting in Fig. 10, i.e., at various distances in the same propagating plane, would help deciphering the main factors.

The comparison of the results at the three hydrophone locations, for a 10 Hz source, a SOFAR channel and a velocity gradient in the crust (case SG; Fig. 11), with the data (Fig. 2) leads to the following observations.

The spectra of simulated T-waves for hydrophones M6 and M8 show the same characteristics as the spectrum of the simulated T-waves for hydrophone M7: 0–15 Hz frequency bandwidth and a Gaussian shape spectrum centered at a frequency lower than the source frequency. The amplitude spectrum of the observed data is broader in the high frequencies (up to 30 Hz) and asymmetric relative to the maximum amplitude frequency at 5–7 Hz.

All the predicted T-wave signals have a duration of about 80–100 s and are shorter than the observed signals (100–120 s). Rise times are shorter for M7 and longer for M6 and M8. Accounting for 3D effects would lengthen the coda signals.

The main T-wave arrivals are well predicted (delays <5 s) by our models for each hydrophone. Precursors are also predicted, however they are more subdued and arrive with a 10 s delay at M6 and M7 and up to 15 s at M8.

Simulated signals at M6 and M7 have similar amplitudes, but higher than those at M8. In Fig. 2, the noise level at M8 looks exaggerated with respect to M6 and M7, suggesting that M8 amplitudes are also exaggerated (perhaps due to a different instrument calibration). These differences probably reflect more efficient conversions in the M6 and M7 cases with a weaker signal at M8 resulting from seafloor depths always deeper than the SOFAR channel axis, particularly in the vicinity of the epicenter (Fig. 3). They may also reflect the differences in the radiation pattern of the source (Fig. 4).

VI. CONCLUSION

This paper demonstrates the ability of the SPECFEM2D code to model T-wave generation and propagation. Modeling T-waves is inherently complex due to the conversion of seismic waves (propagating within the crust) to acoustic waves (propagating within the water layer). The first advantage of SPECFEM2D relative to purely acoustic models is to handle this wave conversion at a realistic crust/water interface, which is highly sensitive to the content of the seismic waves and thus to the crustal parameters. Its second advantage is to consider the source as a moment tensor, which fully defines the radiation pattern of P- and S-waves produced by an earthquake. Its third advantage is its ability to take into account all the environmental parameters of the problem (wave speeds in the water and in the crust, bathymetry) with a good accuracy and potential horizontal variations to handle range-dependent simulations.

Despite the simplifications in our models, for instance in the source shape or in the crustal parameters, SPECFEM2D is able to produce realistic T-wave signals with cigar shapes and durations of 80-100 s, similar to actual data. Furthermore the observed differences with the data may provide insights on the source and the medium.

ACKNOWLEDGMENTS

G. Jamet was supported by a joint Ph.D. grant from the Délégation Générale de l'Armement (DGA) and the University of Brest (UBO). The SPECFEM2D code was run on Caparmor, a massive computing facility common to several research institutions at the westernmost part of Brittany (France). The hydrophone data were provided by Julie Perrot. We wish to thank John Colosi (Associate Editor) and two anonymous reviewers for their insightful comments, which greatly contributed to improve the paper.

Amante, C., and Eakins, B. (**2009**). "ETOPO1 1 arc-minute global relief model: Procedures, data source and analysis," NOAA Technical Memorandum NESDIS NGDC-24 (National Oceanic and Atmospheric Administration, Washington, DC), 19 pp.

Bassin, C., Laske, G., and Masters, G. (**2000**). "The current limits of resolution for surface wave tomography in North America," EOS Trans. Am. Geophys. Union **81**, F897.

Chapman, N. R., and Marrett, R. (**2006**). "The directionality of acoustic T-phase signals from small magnitude submarine earthquakes," J. Acoust. Soc. Am. **119**, 3669–3675.

Cristini, P., and Komatitsch, D. (**2012**). "Some illustrative examples of the use of a spectral-element method in ocean acoustics," J. Acoust. Soc. Am. **131**, EL229–EL235.

de Groot-Hedlin, C., and Orcutt, J. (**2001**). "Excitation of T-phases by seafloor scattering," J. Acoust. Soc. Am. **109**, 1944–1954.

Fox, C., Dziak, R., Matsumoto, H., and Schreiner, A. (**1994**). "Potential for monitoring low-level seismicity on the Juan de Fuca Ridge using fixed hydrophone arrays," Mar. Technol. Soc. J. **27**, 22–30.

Goslin, J., Lourenco, N., Dziak, R., Bohnenstiehl, D., Haxel, J., and Luis, J. (**2005**). "Long-term seismicity of the Reykjanes Ridge (North Atlantic) recorded by a regional hydrophone array," Geophys. J. Int. **162**, 516–524.

Goslin, J., Lourenco, N., Luis, J., Dziak, R., Balanche, A., Brachet, C., Perrot, J., Royer, J.-Y., Simao, N., Haxel, J., and Matsumoto, H. (**2008**). "Cruise MARCHE3/2008 and other cruises of the MARCHE experiment: A three-year hydroacoustic monitoring of the MOMAR section of the MAR at regional scale," Interridge **17**, 7–9.

Jagger, T. (**1930**). "How the seismograph work," Volcano Lett. **21**, 229–232.

Jamet, G., Guennou, C., Guillon, L., and Royer, J.-Y. (**2012**). "Very low frequency wave propagation numerical modeling: Application to T-waves propagation," in *Proceedings of the European Conference on Underwater Acoustics* (Curran, Red Hook, NY), Vol. 34, pp. 1931–1939.

Komatitsch, D., Barnes, D., and Barnes, C. (**2000**). "Wave propagation near a fluid-solid interface: A spectral-element approach," Geophysics **65**, 623–631.

Komatitsch, D., and Tromp, J. (**1999**). "Introduction to the spectral element method for 3D seismic wave propagation," Geophys. J. Int. **139**, 806–822.

Komatitsch, D., and Vilotte, J. (**1998**). "The spectral element method: An efficient tool to simulate the seismic response on 2D and 3D geological structure," Bull. Seismol. Soc. Am. **88**, 368–392.

Linehan, D. (**1940**). "Earthquake in the West Indian region," EOS Trans. Am. Geophys. Union **268**, 1–4.

Okal, E. A. (**2008**). "The generation of T-waves by earthquakes," Adv. Geophys. **49**, 1–65.

Pan, J., and Dziewonski, A. M. (**2005**). "Comparison of mid-oceanic earthquake epicentral differences of travel time, centroid locations, and those determinated by autonomous hydrophone arrays," J. Geophys. Res. **110**, B07302, doi:10.1029/2003JB002785.

Park, M., Odom, R. I., and Soukup, D. J. (**1999**). "Modal scattering: A key to understand oceanic T-waves," Geophys. Res. Lett. **28**, 3401–3404, doi:10.1029/2001GL013472.

Patera, A. (**1984**). "A spectral element method for fluid dynamics: Laminar flow in a channel expansion," J. Comput. Phys. **54**, 468–488.

Stephen, R. A., Pardo-Casas, F., and Cheng, C. H. (**1985**). "Finite-difference synthetic acoutic logs," Geophysics **50**, 1588–1609.

Teague, W. J., Carron, M. J., and Hogan, P. J. (**1990**). "A comparison between the generalized digital environmental model and Levitus climatologies," J. Geophys. Res. **95**, 7176–7183, doi:10.1029/JC095iC05p07167.
Tolstoy, I., and Ewing, M. (**1950**). "The T-phase of shallow-focus earthquakes," Bull. Seismol. Soc. Am. **40**, 25–51.
Tromp, J., Komatitsch, D., and Liu, Q. (**2008**). "Spectral-element and adjoint methods in seismology," Commun. Comput. Phys. **3**, 1–32.
Williams, C. M., Stephen, R. A., and Smith, D. K. (**2006**). "Hydroacoustic events located at the intersection of the Atlantis (30°N) and Kane (23°40'N) transform faults with the Mid-Atlantic Ridge," Geochem. Geophys. Geosyst. **7**, 28 pp.
Yang, Y., and Forsyth, D. W. (**2003**). "Improving epicentral and magnitude estimation of earthquakes from T-phases by considering the excitation function," Bull. Seismol. Soc. Am. **93**, 2106–2122.